An Extended In Situ Cu−K XAFS and XRD Study on the Site Preference and Valence of Copper Ions in $(Mg_{1-x}Cu_x)O$

Nicole Hilbrandt* and Manfred Martin

Darmstadt University of Technology, Institute of Physical Chemistry, Petersenstrasse 20, D-64287 Darmstadt, Germany

Received: November 9, 1998; In Final Form: April 8, 1999

The local environment and valence of copper ions in copper-doped magnesium oxide, $(Mg_{1-x}Cu_x)O$, were investigated under in situ conditions as a function of temperature T, composition x, and oxygen activity a_{O_2}. By comparison of Cu−K extended X-ray absorption fine structure (EXAFS) data with corresponding multiple scattering EXAFS simulations, copper was proven to occupy preferentially magnesium lattice sites. The bivalency and the site preference of copper was inferred from a comparative X-ray absorption near edge structure (XANES) study using standards containing copper in various oxidation states and coordination geometries. Strong similarities between the Fe−K XANES of Fe^{2+} in $(Mg_{1-x}Fe_x)O$ and the discussed Cu−K XANES support these interpretations. Additionally, the Jahn−Teller distortion was estimated to be small at room temperature. As the site preference and valence of copper is not influenced by variation of the experimental conditions, the local thermal expansion around copper in $(Mg_{0.948}Cu_{0.052})O$ was characterized by quantitative EXAFS analysis. The thermal expansions extracted from the nearest and next-nearest radial distribution function coincide with those determined from in situ recorded X-ray diffraction data. Furthermore, the Cu−K step height $\Delta\mu d$ is found to correlate with the lattice parameter a of $(Mg_{0.948}Cu_{0.052})O$, indicating the step height change to be also a measure of thermal expansion.

1. Introduction

Magnesium oxide, MgO, and its derivates, although extensively studied for decades,[1] are still the focus of recent research efforts.[2−5] These compounds represent technically relevant materials widely used as oxide ceramics for high-temperature applications,[1] oxygen sensors,[6] composite materials,[7] or in catalysis as support materials or mixed-oxide catalysts.[8,9] In addition, the structurally simple MgO (NaCl-type, space group $Fm3m$) is often used as model substance to describe the chemical and physical properties of oxide compounds caused by crystal defects. These properties are substantially influenced by the path of synthesis, the (thermodynamic) operating conditions, and the amount of homo- or heterovalent dopant ions. Especially the redox behavior and the site distribution of the dopant within the matrix oxide control macroscopic properties such as ionic and electrical conductivity or catalytic activity depending on the induced point defect structure type. However, the information on the dopant's oxidation degree and site distribution is often not directly accessible.

In the late 40s, the MgO derivate copper-doped magnesium oxide, $(Mg_{1-x}Cu_x)O$, was synthesized and structurally characterized by Rigamonti,[10] and quenched specimens were tested with respect to their catalytic activity[8,9] and optical properties.[11] $(Mg_{1-x}Cu_x)O$ crystallizes in the rock salt structure ($a = 421.14-421.31$ pm at $T = 293$ K and $x \leq 0.1$[12,13]), and according to the $x-T$ phase diagram,[14−16] the magnesium-rich phase ($x < 0.20$) is stable over a wide range of temperature and composition. Although structurally rather simple (both sublattices are cubic face centered), the local environment and valence of the copper dopant might differ from those of the matrix ions, and its nature is still unknown: The valence of copper may vary between +1 and the unusual valence state +3.[11−20] The dopant may substitute magnesium or be distributed within the interstitial sublattice depending on the experimental conditions.[3,21] The existence of a Jahn−Teller distortion around Cu[Ar]d^8 and Cu[Ar]d^9 is also possible at low temperatures ($T < 300$ K) and is controversially discussed in the literature.[8,9,18−20,22]

To systematically and directly investigate the state of copper in $(Mg_{1-x}Cu_x)O$, we have performed in situ Cu−K X-ray absorption experiments over a wide range of temperature ($T = 293-1376$ K), composition ($x < 0.08$), and oxygen activity ($a_{O_2} \leq 0.21$). Both the Cu−K XANES (X-ray absorption near edge structure) and EXAFS (extended X-ray absorption fine structure) regions were analyzed, and different features in the near edge fine structure were tested to extract detailed information about the compound and its thermal behavior. The possible occurrence of a Jahn−Teller distortion was also taken into consideration during these analyses. The study was completed by in situ powder diffraction to test the reliability of the XAFS analysis and to relate long- and short-range order information.

To ensure the homogeneity of the polycrystals within the stability field of the compound, especially at high temperature, this investigation was based on the phase diagram "composition x versus oxygen activity a_{O_2}" ($T = 1373$ K), recorded in a previous study (Figure 1).[23] The solubility of copper in MgO was found to strongly decrease with decreasing oxygen activity. This restricts the a_{O_2} range available for experiments on $(Mg_{1-x}Cu_x)O$. The phase boundary separating the single-phase field of $(Mg_{1-x}Cu_x)O$ from the two-phase field was confirmed by thermogravimetric investigations.[3]

* To whom correspondence should be addressed: Nicole Hilbrandt, Purdue University, Department of Chemistry, 1393 Brown Building, Box 137, West Lafayette, IN 47907-1393. E-mail: nicole@samba.chem.purdue.edu.

10.1021/jp984357p CCC: $18.00
Published on Web 05/20/1999

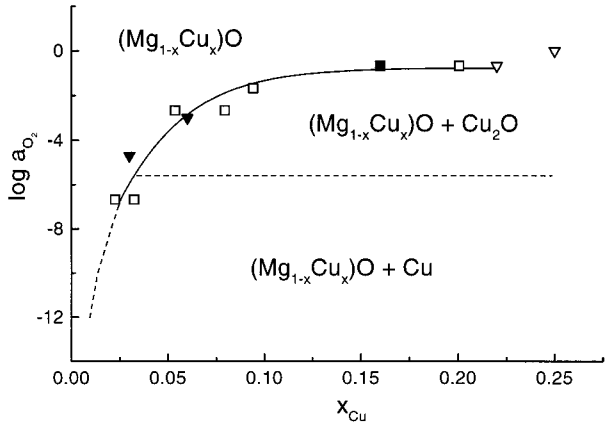

Figure 1. Part of the Mg−Cu−O phase diagram: composition x versus oxygen activity a_{O_2} at the magnesium rich side (T = 1373 K): ▼[3]; ▽[14]; ■;[16] □.[23]

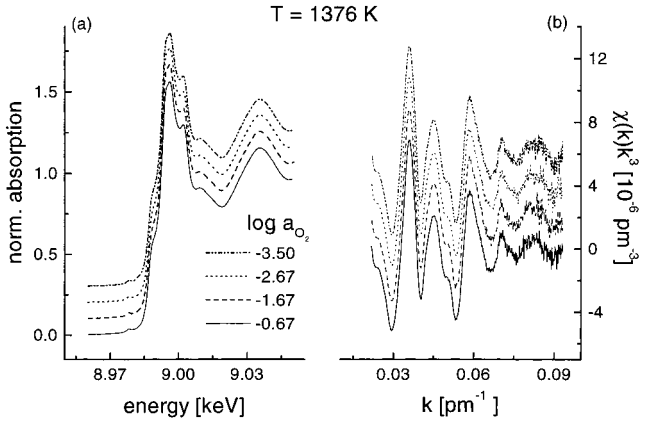

Figure 2. Cu−K XANES (a) and EXAFS (b) of $(Mg_{0.948}Cu_{0.052})O$ after equilibration under various oxygen activities at T = 1376 K. For clarity, the EXAFS are shifted against each other.

2. Experimental Section

Synthesis and Characterization of $(Mg_{1-x}Cu_x)O$. The X-ray absorption and diffraction experiments were carried out on $(Mg_{1-x}Cu_x)O$ polycrystals. These were prepared from mixed, milled, and isostatically compressed oxide powders (MgO − J. Matthey ultrapure 99.99%, CuO − Fluka purriss. p.a. >99%). The compacts were afterwards equilibrated for 10−14 days at T = 1373 K in air within the stability field of copper-doped MgO (Figure 1). The final composition x was determined by electron microprobe analysis (accuracy $\Delta x = \pm 0.001$). All samples (x = 0.027, 0.038, 0.052, 0.075) were homogeneous in concentration. By EDS analysis, no impurities were detected above the resolution limit ($\Delta x/x = \pm 0.001-0.01$). The density of the obtained polycrystals reaches about 85% of the single-crystal density of $(Mg_{1-x}Cu_x)O$[12,13] with typical grain diameters varying between 10 and 25 μm.

XAFS Experiments. Portions of the sintered specimens were polished down to 82−110 ± 1 μm thick slides to be used for in situ XAFS experiments. To ensure that the absorbers contained neither pinholes nor cracks, all samples were light-tested prior to the experiment. The absorption experiments were carried out in a high-temperature furnace ($T_{max} \approx 1500$ K) under continuous gas flow[24] in transition geometry. Temperature stability within ±1 K was guaranteed by a Pt−PtRh10 thermocouple placed near the absorber and coupled with a PID-controlled heating system. During the heating and equilibration period the conditions were established so that the specimen remained in the single-phase field ($a_{O_2} = 0.21$). The experiments were performed either with increasing or decreasing temperature to test reproducibility. The experimental setup was integrated in HASYLAB's nonfocusing bending magnet beamline X1.1 at DESY operating at 4.45 GeV and 60−100 mA. To eliminate higher harmonics, the double-crystal Si(111) monochromator was detuned and stabilized to 50% of the incident intensity I_0 at the absorption edge. The energy was calibrated to the edge position E_0 (first inflection point in the raising edge) of a simultaneously measured Cu reference (Goodfellow, ultrapure, light-tested, 7.8 μm thick) assigning E_0 = 8.9803 keV.[25] N_2-filled ionization chambers were used to detect the photon intensities. Data points in the EXAFS regions were collected at approximately equidistant intervals in k-space, while the XANES spectra were taken in 0.25 eV increments.

XAFS Data Analysis. The data reduction and analysis of the experimental spectra were performed using the software package WinXAS 1.0,[26] based on standard routines for the data reduction of X-ray absorption spectra and on the cumulant expansion technique for data analysis.[27−29] As standards for XAFS analysis Cu (Goodfellow, ultrapure, light-tested, 7.8 μm thick), Cu_2O (Riedel-de-Haen, >98%), CuO (Fluka purriss. p.a. >99%), and self-prepared polycrystalline $(Mg_{1-x}Fe_x)O$ slices[30] were chosen. The absorption spectra of copper and the copper oxides were taken at room temperature using polyethylene-embedded (Merck, Uvasol, for spectroscopy) powders. However, $(Mg_{1-x}Fe_x)O$ was also investigated under in situ conditions (T = 1375 K, $a_{O_2} \leq 10^{-12.3}$) as described above. This procedure ensures that the iron in $(Mg_{1-x}Fe_x)O$ remains divalent and octahedrally coordinated by oxygen ions (for additional material see Supplementary Information, Figure 1S and Figure 2S).[30] Furthermore, multiple scattering cluster calculations within the correlated Debye model[31,32] were performed to simulate the Cu−K EXAFS of copper dissolved in MgO (MgO: space group $Fm3m$, a = 421.12 pm, Θ_D = 743 K[33]), making use of the FORTRAN77 code FEFF6.01.[34−37] The calculated spectra were used to identify the site preference of copper and as theoretical standards in EXAFS analysis.

Powder Diffraction and Data Analysis. For in situ powder diffraction, $(Mg_{0.948}Cu_{0.052})O$ polycrystals were finely ground in an agate mortar and sieved (mesh diameter: 20 μm). The powder was filled into a quartz capillary and placed in a graphite furnace operated under a nitrogen atmosphere. The temperature was controlled with Pt−PtRh10 thermocouples. To avoid recrystallization of the quartz capillaries, the temperature range was restricted to 1000 K. The furnace was placed in a STOE Stadi P diffractometer equipped with a Ge(111) monochromator and a position-sensitive detector (range, 6°; canal distance, 0.02°), and the measurements were performed in Debye−Scherrer mode. For XRD analysis and Rietveld refinement,[38,39] the program FULLPROV was used.

3. Results and Comparative Discussion

Influence of a_{O_2} and x on the Cu−K XAFS (T = 1376 K). By varying the oxygen activity between $a_{O_2} = 0.21$ and values near the phase boundary (Figure 1) at constant temperature and composition ($0.025 < x < 0.075$), copper in the magnesium oxide matrix is expected to be reduced with decreasing oxygen activity. In the same course, the site distribution within the structure should change, because low-valent copper prefers coordination sites with less than six ligands. However, despite several hours of equilibration, the experiments yield a constant, a_{O_2}-independent Cu−K edge position and XANES shape at T = 1376 K (Figure 2a). In addition, no significant influence of the oxygen activity on the EXAFS region can be observed at

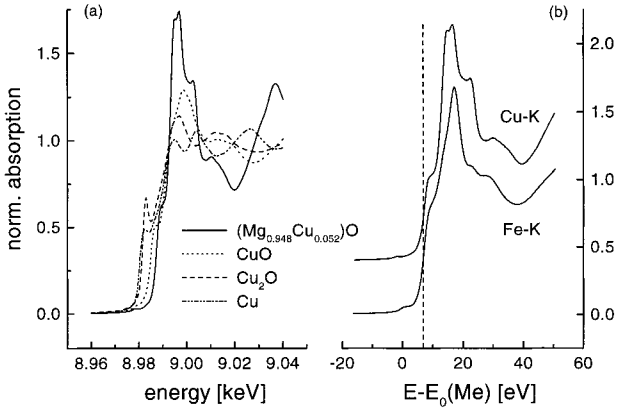

Figure 3. (a) Comparative Cu−K XANES analysis using room temperature standards to determine the valence and coordination geometry of copper in $(Mg_{0.948}Cu_{0.052})O$ ($T = 1376$ K, $a_{O_2} = 0.21$). (b) Comparison between the Fe−K and Cu−K XANES of iron and copper-doped MgO, $(Mg_{1-x}Me_x)O$ ($x_{Fe} = 0.053$ and $x_{Cu} = 0.052$). The energy scale was calibrated to the first inflection points, E_0, of the corresponding metal reference spectra. The dashed line marks E_0 for the Me−K edges.

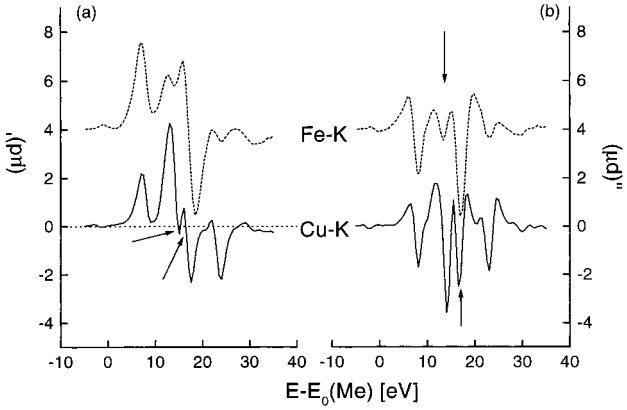

Figure 4. Comparison between the first and second derivatives of the Fe−K and Cu−K XANES of iron and copper-doped MgO, $(Mg_{1-x}Me_x)O$ ($x_{Fe} = 0.053$ and $x_{Cu} = 0.052$). The energy scale was calibrated to the first inflection points, E_0, of the corresponding metal reference spectra.

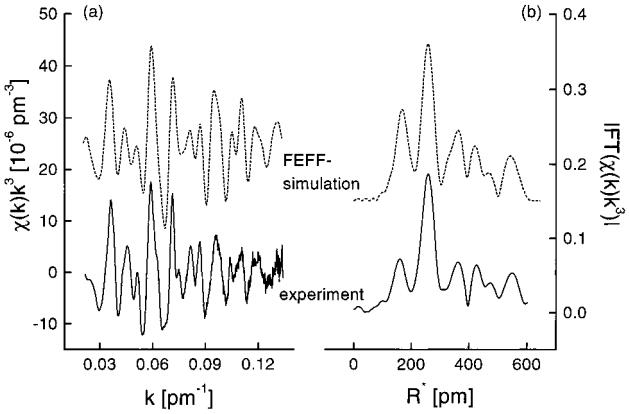

Figure 5. The EXAFS $\chi(k)k^3$ (a) and its Fourier transform (b) for copper in $(Mg_{1-x}Cu_x)O$ at $T = 293$ K either extracted from experimental data, $x = 0.052$, or obtained by multiple scattering EXAFS simulation within the correlated Debye model, $\Theta_D = 743$ K.

given x (Figure 2b). The same invariance of the XAFS features was obtained for different dopant levels. Considering the sensitivity of X-ray absorption spectroscopy, this indicates a constant oxidation state and site occupation of copper in $(Mg_{1-x}Cu_x)O$ within the range of the thermodynamic parameters studied.

To determine the valence and coordination geometry of copper in the MgO matrix, the Cu−K XANES was first compared with standards in which the oxidation state and site distribution of copper is known. In general, the position and shape of different features in the near edge structure are essentially influenced by the effective charge of the absorbing species determined by the absorber's bond characteristics, the coordination geometry, and the formal charge.[40] Within the series of copper-containing standards (Cu, Cu_2O, and CuO) the XANES-shift to higher energy is caused by an increase in formal charge from 0 for Cu to +2 for CuO accompanied by an increase in the number of coordinating oxygen anions from 0 to 4 (Figure 3). Thus, both a higher oxidation state and a higher coordination number of copper could cause the additional edge shift observed at the Cu−K edge of $(Mg_{1-x}Cu_x)O$. As proof for copper in octahedral or slightly distorted octahedral coordination, the weak intensity of the pre-edge peak can be considered. The peak can be assigned to the $1s-3d$ transition, which in the case of an octahedral geometry is dipole-forbidden and quadrupole-allowed because of a lack in p-overlap caused by the neighboring atoms. However, the presence of Cu^{3+} as a majority defect within the system can be ruled out because of the strong similarity between the XANES of copper in $(Mg_{1-x}Cu_x)O$ and of divalent, octahedrally coordinated iron in $(Mg_{1-x}Fe_x)O$[41] and between the derivatives of the XANES of both compounds, as shown in Figure 3b and Figure 4. The shape of the XANES and the peak positions relative to the corresponding metal reference are nearly identical. The peak splitting pattern is also very similar, even within the white line (marked by arrows in Figure 4). Therefore it can be concluded that copper, like iron in the chosen sample, is dissolved as divalent species substituting magnesium in magnesium oxide. In addition, the chemical bond character of both dopants ought to be close to each other, because this parameter also influences the edge and peak positions.

These results coincide with thermogravimetric measurements on the nonstoichiometry δ of $(Mg_{1-x}Cu_x)_{1-\delta}O$.[3] Within the accuracy of the microbalance ($\Delta m = \pm 1\ \mu g$), no mass changes were observed after jumps in a_{O_2} at given x were made. From this behavior it was concluded that the copper balance is dominated by the incorporation of divalent copper on magnesium lattice sites.

Details on the Local Environment of Copper ($T = 293$ K). To get a more detailed picture of the valence and local environment of copper within the host lattice, the following discussion will be focused on $(Mg_{0.948}Cu_{0.052})O$. As shown in Figure 5, the k^3-weighted EXAFS and the corresponding Fourier transform of copper in $(Mg_{0.948}Cu_{0.052})O$ can be excellently reproduced by EXAFS simulations applying the FEFF6.01 code, although these data were recorded ex situ (for comparison with in situ measurements see Figure 6). The calculations were based on a structure unit (= cluster) of MgO ($a = 421.12$ pm) constructed around a copper atom. The copper atom occupies a magnesium lattice site, i.e., the cluster shows O_h symmetry. Single and multiple scattering paths involving at maximum four backscattering centers up to $R_{max} = 600$ pm were considered. Thermal disorder was approximated by the correlated Debye model ($\Theta_D = 743$ K).

At low temperature, however, deviations from the ideal (symmetric) distribution might influence the radial pair distribution function around copper in MgO as well as the electronic structure of the dopant. Within the crystal field of the MgO lattice, the degenerated $3d$ states of Cu^{2+} (electronic configuration $[Ar]d^9$) can split fourfold upon reduction of the site symmetry from O_h to D_{4h} or D_{2h}. Such tetragonal splitting in

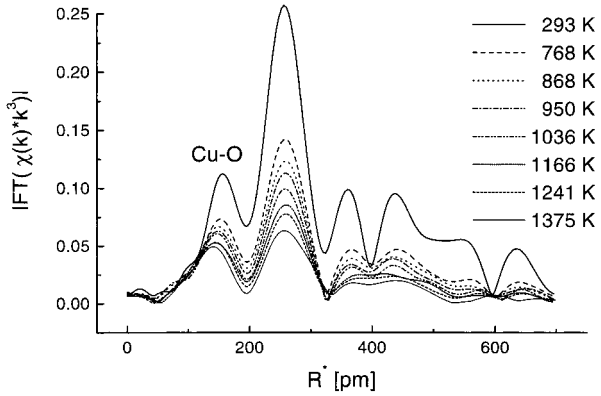

Figure 6. Temperature dependence of the Fourier transformed Cu−K EXAFS $\chi(k)k^3$ of copper in $(Mg_{0.948}Cu_{0.052})O$ between $T = 293$ and 1376 K ($a_{O_2} = 0.21$).

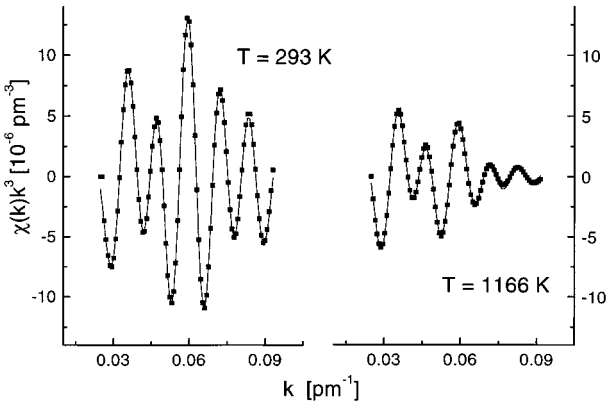

Figure 7. Comparison between experimental EXAFS data (−) and fit (■) applying the cumulant expansion technique at $T = 293$ and 1166 K ($(Mg_{1-x}Cu_x)O$, $x = 0.052$).

its extreme is visible in CuO: Copper is coordinated in a planar orientation by four oxygen ions at a distance of 196 pm and by two axial oxygen ions at 266 pm.[42] With respect to copper in magnesium oxide, the presence of a Jahn−Teller distortion was discussed with much controversy, but its nature remains unsolved.[8,9,18−20,22] According to theoretical XANES studies on the multiple scattering within CuO_6 units,[43,44] a tetragonal Jahn−Teller distortion causes a splitting of the white line, as observed for tenorite, if the axial and equatorial Cu−O bonds differ by 30 pm or more. The white line of the Cu−K XANES of $(Mg_{0.948}Cu_{0.052})O$ is also split, but as depicted in Figure 4, the same effect was found for octahedrally coordinated Fe^{2+} in MgO. An additional splitting was not observed. Thus, a large Jahn−Teller effect caused by bond differences of $\Delta R \geq 30$ pm can be excluded. Smaller distortions can be studied by analyzing the frequency behavior of the EXAFS amplitude. If the first peak in the Fourier transform is composed by an oxygen backscatterer whose Cu−O distance differs by ΔR, a beat node is expected to occur at $k = 0.5\ \pi/\Delta R$.[45] However, as no beat node is observed within the data range ($k_{max} = 0.14$ pm^{-1}) after backtransformation of the first peak, the presence of a distortion between 11 and 30 pm can also be ruled out. A multiple shell EXAFS analysis using either theoretical or experimental Cu/O amplitude and phase functions to describe the first peak in the Fourier transform corroborate these results. Considering the experimentally available data range, the distribution function of the first coordination sphere can be always represented by an undisturbed CuO_6 unit ($R_1 = 210.4 \pm 1.0$ pm[46]).

Referring to our EXAFS simulations, the structure of the second peak between 200 and 300 pm (Figure 5) is more complex. Besides Cu−Me (Me = Mg and Cu) and Cu−O backscattering from the second ($N = 12$) and third ($N = 8$) coordination shell, Cu−O−Me triple scattering also contributes to the EXAFS signal. Fitting all parameters required for such a detailed EXAFS analysis, especially with respect to higher temperatures, is however impossible. To overcome this restriction and to determine the type, number, and distance of backscatterers at $R_2 \cong a/2^{1/2}$, the complex-structured peak was considered to be composed of only one Cu−Me coordination shell. The amplitude and phase functions were extracted from simulated EXAFS spectra consisting of either 12 Mg or 12 Cu backscatterers in the second coordination shell. These spectra were Fourier transformed over the same data range as the experimental data and backtransformed between 200 and 300 pm before the phase and amplitude functions were calculated. The advantage of this procedure lies in the accurate determination of the Cu−Me distance once the type and number of backscatterers are defined. As inferred from a detailed analysis of simulated spectra as a function of T, the systematic error in R is restricted to ± 0.5 pm. Of course the absolute values of the Debye−Waller factor, and with respect to the high-temperature analysis, the third cumulant C_3 cannot be obtained by this technique. Besides the temperature dependence of the shell under study, both the amplitude and phase functions also include the thermal evolution of the multiple scattering paths and the next Cu−O shell ($N = 8$). For this reason, the thermal evolution of these parameters will not be further discussed.

Taking into account the phase and amplitude functions, determined in the way described above, the second peak in the Fourier transform around copper in $(Mg_{0.948}Cu_{0.052})O$ can be represented in a first approximation by 12.0 (± 0.5) magnesium backscatterers at $R_2 = 296.9 \pm 1.0$ pm. A refined constrain analysis yields 11.6 (± 0.6) Mg and 0.4 (± 0.3) Cu at R_2 (constrains: $N_2 = N_{Mg} + N_{Cu} = 12$, $R_2 = R_{Mg} = R_{Cu}$). This indicated that copper is statistically dissolved within the magnesium lattice. Further shells corresponding to additional copper species cannot be resolved because of parameter correlations.

Quantitative EXAFS Analysis as a Function of Temperature.[47] The increase in temperature at constant oxygen activity ($a_{O_2} = 0.21$) is accompanied by a strong decrease in magnitude of the EXAFS oscillations, restricting the available data range for analysis to $k_{max} = 0.095$ pm^{-1}. In addition, the peaks in the Fourier transform broaden and shift to lower R^* values, as is clearly visible in Figure 6 for the first peak related to the Cu−O bond. The observed trends can also be reproduced in reverse order by reducing the sample's temperature. A conventional two-shell EXAFS analysis ($R^* = 100-300$ pm, $k = 0.022-0.095$ pm^{-1}) within the harmonic approach yields a decrease in coordination number and interatomic distances with increasing temperature ($T = 293-1376$ K). Furthermore, the quality of the fit in either R^*- and k-space worsens with T. Especially at high k, the fitted frequency behavior strongly differs from the experimental data. Both observations indicate the need for the consideration of anharmonic vibrations and asymmetric pair potentials to correctly describe the Debye−Waller damping and thermal expansion with increasing temperature.

To account for the deviation from harmonic behavior, the cumulant expansion technique[28,29] was applied using the phase and amplitude functions extracted as discussed in the previous section. The fit was found to fully reproduce the frequency pattern considering cumulants up to C_3, as shown in Figure 7. Over the whole temperature range, the first two peaks of the Fourier transform can be described via one CuO_6 and one $CuMg_{12}$ unit ($\Delta N = \pm 0.5$).

TABLE 1: Thermal Expansion Derived from First and Second Shell EXAFS Analysis and XRD Measurement on $(Mg_{0.948}Cu_{0.052})O$ at $T > 600$ K and from XRD Literature Data on MgO [33]

$(R_1^0)^{-1}(dR_1/dT)$	$(R_2^0)^{-1}(dR_2/dT)$	$(a^0)^{-1}(da/dT)$	$(a^0)^{-1}(da[\mathrm{MgO}]/dT)$ [33]
$1.5\ (\pm 0.1) \times 10^{-5}\ K^{-1}$	$1.4\ (\pm 0.1) \times 10^{-5}\ K^{-1}$	$1.65\ (\pm 0.25) \times 10^{-5}\ K^{-1}$	$1.6\ (\pm 0.1) \times 10^{-5}\ K^{-1}$

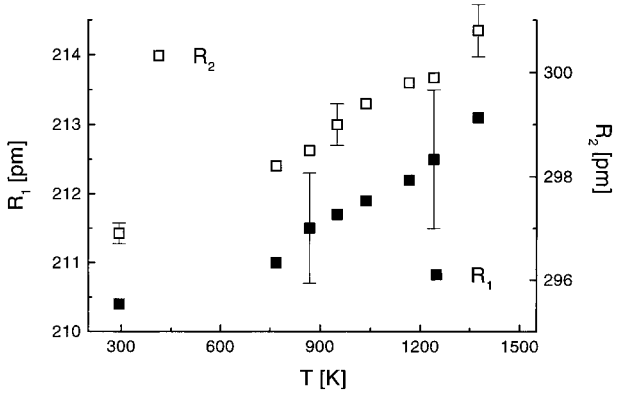

Figure 8. Cu−O and Cu−Mg bond length as a function of temperature derived from EXAFS analysis (for procedure, see text). The fitting errors, and not the systematic errors,[46] are depicted as error bars.

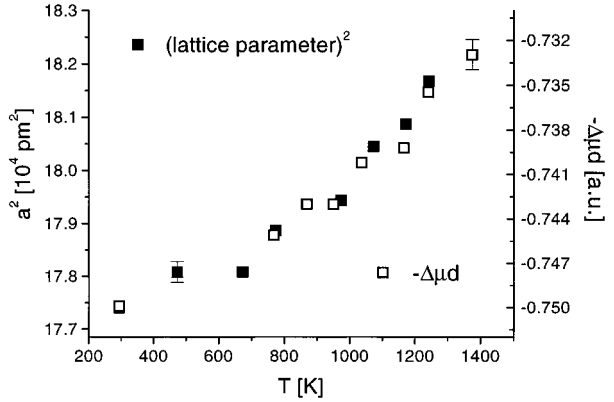

Figure 9. Correlation of the Cu−K step height $\Delta\mu d$ and the lattice parameter a as a function of temperature T for $(Mg_{0.948}Cu_{0.052})O$.

Above 600 K the interatomic distances between copper and oxygen, R_1, and copper and magnesium, R_2, increase linearly with T (Figure 8). Their ratio satisfies $R_2(T)/R_1(T) \cong 2^{1/2}$, as expected for the lattice geometry of the NaCl-type matrix lattice. This indicates, within the discussed errors, small or negligible distortions around the Cu^{2+} dopant ion, whose ionic radius in octahedral coordination is only slightly larger than that of Mg^{2+} ($r(Cu^{2+}) = 73$ pm, $r(Mg^{2+}) = 72$ pm[48,49]). Furthermore, the observed increase in the Cu−O distance is related to the increase in the Debye−Waller factor and the third cumulant C_3 of the first coordination shell (see Supplementary Information, Figure 3S). These terms determine the force constant and the anharmonicity of the pair potential responsible for thermal expansion.[50] A more detailed analysis of the potential and bond characteristics will be given in due course.

Along with the analysis of the temperature dependence of the local environment of copper in air, the data recorded at different oxygen activities ($T = 1376$ K) were also analyzed. The EXAFS parameters ($R_1 = 213.1 \pm 1.0$ pm, $\sigma^2 = 240 \pm 40$ pm^2, $C_3 = 2700 \pm 500$ pm^3, $R_2 = 300.8 \pm 1.0$ pm) coincide with those obtained in air ($a_{O_2} = 0.21$), which indeed indicates no change in the site preference or valence of copper in magnesium oxide.

Combined Cu−K XANES and X-ray Diffraction Analysis on $(Mg_{0.948}Cu_{0.052})O$. For copper-doped magnesium oxide, either a negligible or a linear dependence of the lattice parameter a on the dopant level x was reported ($T = 298$ K, $x < 0.075$).[11−13] On the basis of these data, taking either Vegards's law into account or referring to the Shannon ionic radii,[48,49] the Cu−O bond length can be estimated to $R_1 \cong 211.4-211.6$ pm. These values are only about 0.8−1.0 pm higher than the Mg−O distance in MgO. Considering, in addition, a lattice relaxation with R^{-2}, as proposed for isovalent dopants,[51] the Cu−Mg distance and the higher distant coordination spheres should not significantly deviate from those of the matrix lattice.

The EXAFS results obtained in the previous sections show that the difference between the local environment of copper and those of the matrix cations is small. Therefore, the temperature dependence of the first nearest-neighbor distances, dR_1/dT and dR_2/dT, ought to be calculated from the temperature dependence of the lattice (long-range order) parameter da/dT. The results, in comparison with the thermal expansion of pure MgO derived from literature data,[33] are summarized in Table 1. To ensure direct comparability, the values are normalized to a^0 and R^0 at $T = 0$ K, obtained by extrapolation of the corresponding data to 0 K. Within the errors of analysis, the normalized thermal expansion coefficients coincide. Doping with $x = 0.052$ does not influence the temperature behavior of the crystal with respect to pure MgO, implying strong similarities between the interatomic forces of Cu^{2+} and Mg^{2+}.

Apart from the discussed changes in the lattice constant a, the thermal expansion of the crystal can be derived from the temperature dependence of the XANES: According to Beer's law, the step height of the edge jump before normalization, $\Delta\mu d$,[52] is directly proportional to the product of the number of absorbing species per sample volume, n/V, and the sample's thickness d. As the dopant fraction $x = 0.052$ of the oxide remains constant[53] during the heating and equilibration periods, the decrease of $\Delta\mu d$ with T is attributed to the change of the sample area (perpendicular to the X-ray beam) because of thermal expansion of the crystal. Therefore $\Delta\mu d(T)$ must also correlate with the dimensions of the unit cell. Figure 9 depicts the temperature evolution of $-\Delta\mu d$ and a^2. The expected linear correlation between $\Delta\mu d$ and a^{-2} is observed, and the scaling relation between both parameters relative to $\Delta\mu d$ at $T = 293$ K is given by[54]

$$\frac{\Delta\mu d(T)}{\Delta\mu d(293\ \mathrm{K})}\, a^2(T) = a^2(298\ \mathrm{K}) = 177620\ (\pm 80)\ \mathrm{pm}^2 \tag{1}$$

In contrast to the conventional understanding of XAFS, being a technique to characterize the short-range order around an absorbing species, the analysis of the step height $\Delta\mu d$ demonstrates that, by all means, the unnormalized XANES also includes information about long-range order parameters of the system under study.

4. Conclusion

This study emphasizes the possibility of extracting reliable element-specific structural parameters at high temperatures, although the accuracy of analysis is strongly influenced by Debye−Waller damping and the restriction in data space: Within a temperature range of $T = 293-1376$ K, the site preference and formal valence of copper in $(Mg_{1-x}Cu_x)O$ persists upon varying the experimental parameters x and a_{O_2}. The host

lattice preferentially stabilizes divalent copper ions in nearly undisturbed octahedral coordination on magnesium lattice sites. Apart from this, the presence of minority defects such as monovalent copper distributed on magnesium or interstitial lattice sites cannot be excluded solely based upon XAFS studies. Although element-specific, this technique does not allow the resolution of dopant species with atomic fractions smaller than 1−10% (depending on the composition of the compound and the experimentally available data range at given temperature). Especially at high T ($T > 1200$ K), these results coincide with the conclusions drawn in ref 3, where the nonstoichiometry of $(Mg_{1-x}Cu_x)O$ was investigated thermogravimetrically. Within the accuracy limits of the method, no change in the nonstoichiometry was found as a function of a_{O_2}.

These results open the possibility of studying the physics of this system. Because of the stable copper valence and an unchanged local environment, the system is an ideal candidate for the investigation of bond dynamic effects, as previously done for adsorbates on surfaces,[50,55,56] over a wide range of temperature. This conclusion is supported by the fact that the local thermal expansion around copper in $(Mg_{0.948}Cu_{0.052})O$ can be characterized by quantitative EXAFS analysis and related to in situ recorded X-ray diffraction data. A detailed discussion will be presented in a forthcoming publication. Furthermore, the Cu−K step height $\Delta\mu d$ was found to correlate linearly with the inverse of the cubic lattice parameter, $1/a^2$, of $(Mg_{0.948}Cu_{0.052})O$. This means the change of $\Delta\mu d$ was introduced as a measure of thermal expansion. The same approach should be applicable to studies on the influence of the overall pressure p.

Acknowledgment. We thank Dr. M. Wiesmann for his efforts in XRD data acquisition and analysis. These investigations were financially supported by the Deutsche Forschungsgemeinschaft. N.H. is grateful to the Friedrich Ebert Foundation and Alexander von Humboldt Foundation for a fellowship.

Supporting Information Available: Oxidation degree of iron in $(Mg_{1-x}Fe_x)O$ as a function of T, a_{O_2}, and x, derived from a known point defect model. Temperature evolution of the cumulants of the Cu-O (σ^2 and C_3) and Cu-Mg (R and σ^2) bond as obtained by a two-shell EXAFS analysis. This material is available free of charge via the Internet at http://pubs.acs.org.

References and Notes

(1) (a) Kingery, W. D. *Structure and Properties of MgO and Al_2O_3 Ceramics: Proccedings of an International Symposium*; American Ceramics Society: Columbus, 1984. (b) Kingery, W. D.; Bowen, H. K.; Uhlmann, D. R. *Introduction to ceramics*, 2nd ed.; Wiley & Sons: New York, 1976.

(2) Schmalzried, H.; Backhaus-Ricoult, M. *Prog. Solid State Chem.* **1992**, *22*, 1.

(3) Krafft, K. N. Ph.D. Thesis, University of Hannover, 1994.

(4) Zimnol, M.; Graff, A.; Sieber, H.; Senz, S.; Schmidt, S.; Mattheis, R.; Hesse, D. *Solid State Ionics* **1997**, *95*, 1.

(5) Hilbrandt, N.; Wasserman, S. R.; Martin, M. *Solid State Ionics* **1998**, *101−103*, 431.

(6) Valverde, N. *J. Am. Ceram. Soc.* **1985**, *68*, 657.

(7) Reppich, B. *Mater. Sci. Eng.* **1975**, *19*, 51.

(8) Ueda, W.; Yokoyama, T.; Moro-Oka, Y.; Ikawa, T. *Chem. Lett.* **1985**, 1059.

(9) Asakura, K.; Iwosawa, Y. Mater. *Chem. Phys.* **1988**, *18*, 499.

(10) Rigamonti, R. *Atti. Accad. naz. Lincei* **1947**, *2*, 446.

(11) Schmitz-Dumont, O.; Fendel, H. *Monatsh. Chem.* **1965**, *96*, 495.

(12) Schmahl, N. G.; Barthel, J.; Eikerling, G. F. *Zeitsch. Angew. Allgem. Chem.* **1964**, *332*, 230.

(13) Schmahl, N. G.; Eikerling, G. F. *Z. Phys. Chem., NF* **1968**, *62*, 268.

(14) Gadalla, A. M. M.; White, J. *Trans. Brit. Ceram. Soc.* **1964**, *63*, 119.

(15) Ust'yantsev, V. M.; Bessonov, A. F.; Ust'yantseva, I. A. *Zurnal Fiziceskoj Chimii* **1966**, *40*, 3099.

(16) Ust'yantsev, V. M. *Tr. Vost. Inst. Ogneuporov* **1973**, *13*, 262.

(17) Orton, J. W.; Auzins, P.; Griffiths, J. H. E.; Wertz, J. E. *Proc. Phys. Soc.* **1961**, *78*, 554.

(18) Oku, M.; Hirokawa, K. *J. Electron Spectrosc. Relat. Phenom.* **1977**, *10*, 103.

(19) Pascual, J. L.; Seijo, L.; Barandiarán, Z. *J. Chem. Phys.* **1993**, *98*, 9715.

(20) There are only few oxide compounds in which copper is expected to be trivalent, e.g., Akeyama, K.; Kuroda, H. *Jpn. J. Appl. Phys. Supplements* **1993**, *32*, 98.

(21) Backhaus-Ricoult, M.; Hagère, S. *Philos. Mag. A* **1993**, *67*, 1471.

(22) Asakura, K.; Iwasawa, Y.; Kuroda, H. *J. Phys. Colloq. C8, Suppl.* **1986**, *12*, 317.

(23) Hilbrandt, N. Diploma Thesis, University of Hannover, 1993.

(24) Mechanically premixed air/N_2 and CO/CO_2 gas mixtures were used.

(25) Bearden, J. A.; Burr, A. F. *Rev. Mod. Phys.* **1967**, *39*, 125.

(26) Ressler, Th. *J. Phys. IV France, Suppl.* **1997**, *7*, C2−269.

(27) Koningsberger, D. C.; Prins R., Eds. *X-ray absorption: Principles, applications, techniques of EXAFS, SEXAFS and XANES*; Wiley & Sons: New York, 1988.

(28) Bunker, G. *Nucl. Instrum. Methods* **1983**, *207*, 437.

(29) Tranquada, J. M.; Ingalls, R. *Phys. Rev. B* **1983**, *28*, 3520.

(30) Hilbrandt, N. Ph.D. Thesis, TH Darmstadt, 1997. Hilbrandt, N.; Martin, M. *Ber. Bunsen Gesell. Phys. Chem.* **1998**, *102*, 1747.

(31) Sevillano, E.; Meuth, H.; Rehr, J. J. *Phys. Rev. B* **1979**, *20*, 4908.

(32) Crozier, E. D.; Rehr, J. J.; Ingalls, R. In ref 27, chapter 9.

(33) Landolt-Börnstein *Zahlenwerte und Funktionen aus Naturwissenschaft und Technik*; Springer: Berlin, 1979.

(34) Mustre de Leon, J.; Rehr, J. J.; Zabinsky, S. I.; Albers, R. C. *Phys. Rev. B* **1991**, *44*, 4146.

(35) Rehr, J. J.; Mustre de Leon, J.; Zabinsky, S. I.; Albers, R. C. *J. Am. Chem. Soc.* **1991**, *113*, 5135.

(36) Rehr, J. J. *Jpn. J. Appl. Phys., Suppl.* **1993**, *32* (2), 8.

(37) Zabinsky, S. I.; Rehr, J. J.; Ankudinov, A.; Albers, R. C.; Eller, M. J. *Phys. Rev. B* **1995**, *52*, 2995.

(38) Rietveld, H. M. *J. Appl. Crystallogr.* **1969**, *2*, 65.

(39) Wölfel, E. R. *Theorie und Praxis der Röntgenstrukturanalyse*, 3rd ed.; Vieweg: Braunschweig-Wiesbaden, 1987.

(40) Shrivastava, U. C.; Nigam, H. L. *Coord. Chem. Rev.* **1972**, *9*, 273.

(41) The valence and site distribution of iron in $(Mg_{1-x}Fe_x)O$ was studied in detail; see ref 30. The presence of Fe^{3+} in various lattice sites can be ruled out.

(42) Tröger, L.; Arvanitis, D.; Rehr, J. J.; Lederer, T.; Yokoyama, T.; Baberschke, K.; Zschech, E. *Jpn. J. Appl. Phys.* **1992**, *32* (2), 137.

(43) Garcias, J.; Benfatto, M.; Natoli, C. R.; Bianconi, A.; Fontaine, A.; Tolentino, H. *Chem. Phys.* **1989**, *132*, 295.

(44) Garcia, J.; Bianconi, A.; Benfetto, M.; Natoli, C. R. *J. Phys. Colloq. C8, Suppl.* 12 **1986**, 49.

(45) Teo, B. K. *EXAFS: Basic principles and data analysis, Inorganic Chemistry Concepts 9*, Springer: Berlin, 1986.

(46) Besides the error in fitting of 0.5−1 pm, the use of either experimental or theoretical standards accompanied by the quality of data induces an additional systematical error of 1−2 pm depending on the analyzed data range.

(47) The values for R, discussed in the following section, are already corrected by $\sigma^2/2$.

(48) Shannon, R. D.; Prewitt, C. T. *Acta Crystallogr. B* **1969**, *25*, 925.

(49) The Shannon radii are isotropic, averaged ionic radii, i.e., they are defined for undisturbed coordination geometries, not nescessarily fulfilled for d^9 systems. See Norrestam, R. *Z. Kristallogr.* **1994**, *209*, 99.

(50) Rabus, H. Ph.D. Thesis, FU Berlin, 1991.

(51) Dollase, W. A. *Phys. Chem. Mineral.* **1980**, *6*, 295.

(52) In XANES deconvolution analysis, the edge jump is represented by an arctan function to describe the absorption of the studied core electron to the continuum. The step height $\Delta\mu d$ of the edge jump is given by the difference between both legs of the arctan function. Its value is given by $\Delta\mu d = \Delta\mu_{edge} cd$, where c is the concentration of the absorbing species and d the sample's thickness.

(53) Via a long-time study of $\Delta\mu d$ at high temperature ($T = 1376$ K), a slight evaporation of copper was observed. The average rate of evaporation at $T = 1376$ K is estimated to $dx/dt = 0.00007(3)$/h. Therefore, the observed decrease in $\Delta\mu d$ is only weakly influenced by evaporation, especially as the time required for this experiment is small compared to that necessary to resolve evaporation by XAFS. In addition, no sintering effects were observed.

(54) The same type of relation is found by plotting the normalized edge jump either versus R_1^{-2} or R_2^{-2} obtained by EXAFS analysis. Relating these values to the lattice parameter results in an averaged a^2 (293 K) = 177040 (± 100) pm^2. This again demonstrates the reliability of the described analysing procedures discussed in the course of the paper.

(55) Lederer, T.; Arvanitis, D.; Comelli, G.; Tröger, L.; Baberschke, K. *Phys. Rev. B* **1993**, *48*, 15390.

(56) Yokoyama, T.; Satsukawa, T.; Ohta, T. *Jpn. J. Appl. Phys.* **1989**, *28*, 1905.